In Situ Experimental Evidence for a Nonmonotonous Structural Evolution with Composition in the Molten $LiF-ZrF_4$ System

Olivier Pauvert,*[,†,‡] Didier Zanghi,[†,‡] Mathieu Salanne,[§,∥] Christian Simon,[§] Aydar Rakhmatullin,[†,‡] Haruaki Matsuura,[†,⊥,#] Yoshihiro Okamoto,[▽] François Vivet,[†,‡] and Catherine Bessada[†,‡]

Conditions Extrêmes: Matériaux Haute Température et Irradiation, CNRS, 1D avenue de la Recherche Scientifique, F-45071 Orléans cedex 2, France, Université d'Orléans, Avenue du Parc Floral, BP 6749, F-45067 Orléans cedex 2, France, UPMC Université Paris 06, UMR 7195, PECSA, F-75005 Paris, France, CNRS, UMR 7195, PECSA, F-75005 Paris, France, STUDIUM, 3D avenue de la Recherche Scientifique, F-45071 Orléans cedex 2, France, Research Laboratory for Nuclear Reactors, Tokyo Institute of Technology, 2-12-1 Meguro-ku, Tokyo 152-8550, Japan, and Quantum Beam Science Directorate, Japan Atomic Energy Agency, Shirakata-Shirane 2-4, Tokai-Mura, Ibaraki 319-1195, Japan

Received: December 27, 2009; Revised Manuscript Received: April 6, 2010

We propose in this paper an original approach to study the structure of the molten $LiF-ZrF_4$ system up to 50 mol % ZrF_4, combining high-temperature nuclear magnetic resonance (NMR) and extended X-ray absorption fine structure (EXAFS) experiments with molecular dynamics (MD) calculations. ^{91}Zr high-temperature NMR experiments give an average coordination of 7 for the zirconium ion on all domains of composition. MD simulations, in agreement with EXAFS experiments at the K-edge of Zr, provide evidence for the coexistence of three different Zr-based complexes, $[ZrF_6]^{2-}$, $[ZrF_7]^{3-}$, and $[ZrF_8]^{4-}$, in the melt; the evolution of the concentration of these species upon addition of ZrF_4 is quantified. Smooth variations are observed, apart from a given composition at 35 mol % ZrF_4, for which an anomalous point is observed. Concerning the anion coordination, we observe a predominance of free fluorides at low concentrations in ZrF_4, and an increase of the number of bridging fluoride ions between complexes with addition of ZrF_4.

I. Introduction

When two ionic substances are mixed, some compounds with different stoichiometries can form in the solid phase and be easily identified. This contrasts with the molten state at high temperature for which very little is known on the local structure. This lack of knowledge is due to the difficulty of conducting spectroscopy or diffraction experiments in such media. Most often, it was believed that each particular ionic species could only bind a given number of neighboring counterions. This first solvation shell has been described in some systems by techniques such as Raman spectroscopy.[1,2] The use of molecular dynamics (MD) simulations somehow modified the initial picture.[3,4] In the case of molten salts, and especially of the molten chlorides, it was shown unambiguously that multivalent cationic species were present with various solvation shell structures, depending on the number of halide species available (the chloroacidity in the case of molten chlorides) and on the chemical nature of the other cations of the melt. This picture was later confirmed by the introduction of some new in situ characterization at high temperature, namely, the nuclear magnetic resonance (NMR)[5] and the extended X-ray absorption fine structure (EXAFS).[6] Both techniques are sensitive to the local environment around a given element. It is well-known that structural aspects can strongly influence the physicochemical properties, and a complete description enabling the determination of quantities like the viscosity, the heat capacity, or the thermal conductivity, inter alia, on wide ranges of molten salts compositions, still has to be developed.

In general, the structural description of molten chlorides is more complete than the one of molten fluorides since experiments could more easily be performed in this media. However, it is important to determine such chemical aspects in the case of molten fluoride mixtures, because of their use in different industrial processes, in metallurgy or in nuclear energy applications, as in the case of the molten salt fast reactor (MSFR). The MSFR is one of the six promising future nuclear reactor concepts promoted by the Generation IV international forum. This reactor presents several advantages, notably concerning safety, environment, and efficiency of the fission reaction.[7,8] The studies about molten salts-based reactors began during the 1950s and 1960s in the Oak Ridge National Laboratory (USA). In this concept, the choice of the salt is indeed very important. The system, in which the fuel is dissolved, has to offer excellent neutronic conditions, a good thermal stability and a good ability to dissolve actinides or fission products.[9] Different mixtures have been proposed,[10,11] such as $NaF-ZrF_4-UF_4$ or $LiF-BeF_2-ZrF_4-UF_4$ but $LiF-ThF_4/UF_4$ is now the reference system.[12,13]

Each element produced by the fission reactions will influence the thermochemical properties. It is thus very important to understand how the molten mixture is organized, and to characterize the different species involved in the molten phase. The experimental study of such systems is difficult because of the combination of radioactive risks and molten fluoride

* To whom correspondence should be addressed. E-mail: pauvert@cnrs-orleans.fr.
† Conditions Extrêmes: Matériaux Haute Température et Irradiation, CNRS.
‡ Université d'Orléans.
§ UPMC Université Paris 06.
∥ CNRS.
⊥ STUDIUM.
Tokyo Institute of Technology.
▽ Japan Atomic Energy Agency.

10.1021/jp912195j
Published on Web 04/27/2010

corrosiveness. We propose here a systematic study of a model system without a radioactive element in a wide range of compositions. The objective is to establish some general laws on the chemical and structural behavior in such ionic systems. Because zirconium is an important nuclear fission product of the MSFR, we have chosen to study zirconium fluoride and its mixtures with lithium fluorides.

Due to their strong reactivity at high temperature, and their sensitivity to moisture and oxygen, experiments involving molten fluorides are extremely difficult, therefore requiring some specific developments. Different studies were carried out on molten zirconium fluoride-based system, using mainly Raman spectroscopy. Toth et al.[14] investigated the molten $LiF-NaF-ZrF_4$ system to characterize the different zirconium-based species for several compositions. They found direct evidence for the octahedral $[ZrF_6]^{2-}$ species by comparing the spectra obtained in the melts and in crystalline Li_2ZrF_6. The existence of $[ZrF_7]^{3-}$ and $[ZrF_8]^{4-}$ was also suggested by analogy with previous results on dilute UF_4 in $LiF-BeF_2$ solutions. No conclusion could arise about the presence of bridging fluorines in this study. Dracopoulos et al. investigated different $AF-ZrF_4$ systems ($A^+ = Li^+, K^+, Cs^+$), with the same technique.[15] The 6-fold and 7-fold coordinated species were shown to predominate in the melt. Interpreting the spectral trends observed similarly as in molten chloride systems, they concluded that the species formed small chains connected by their corners and/or their edges.

The thermodynamic aspects have also been studied and discussed. Using high-temperature calorimetry, Hatem et al. measured the enthalpies of formation of different $AF-ZrF_4$ systems ($A^+ = Li^+, Na^+, K^+, Rb^+$).[16] For all systems, negative enthalpies of mixing were deduced from these measurements. This exothermic reaction was explained by the formation of Zr-based anionic complexes. A physical thermodynamic model, introduced by Grande et al. and based on the coexistence of different Zr-based complexes ($[ZrF_6]^{2-}$, $[ZrF_7]^{3-}$, and $[ZrF_8]^{4-}$) in the melt, was able to reproduce the later data.[17]

We propose in this paper a new approach for the study of the structure of the molten $LiF-ZrF_4$ system, to establish which zirconium-based species are present in the melt, and how the molten system is organized. Our approach is based on a combination of in situ NMR and EXAFS experiments supported by molecular dynamics (MD) simulations. The NMR and EXAFS spectroscopies allow the observation of the local structure of a given nucleus in solid or liquid phases, to obtain information about its coordination, the nature of its first neighbors, and what kind of complexes are present in the system. MD simulations can quantitatively be compared to EXAFS oscillations. The comparison with NMR data is for the moment more qualitative. The three techniques support the existence of structural changes in the zirconium first solvation shell with composition. Smooth variations are observed, except at one given composition for which the octahedral $[ZrF_6]^{2-}$ concentration increases importantly.

II. Experiments and Calculations

Samples have been prepared and packed in a glovebox under a dried argon atmosphere. Different compositions have been prepared by mixing β-ZrF_4 purchased from Neyco (99.99% pure of other metallic species) with LiF purchased from Sigma Aldrich (99.9% pure). Compositions extend from 0 to 50 mol % ZrF_4, with a step of 5 mol %. Due to the risk of sublimation of ZrF_4 upon heating, we have limited the ZrF_4 content in our compositions to 50 mol %. Melting points of the different samples were measured by differential scanning calorimetry (DSC). The liquidus temperatures are in good agreement with the phase diagrams reported in the literature.[18,19]

A. NMR. NMR experiments were performed on a Bruker Avance 400 NMR spectrometer (corresponding to a magnetic field of 9.4 T). This spectrometer operates at frequencies of 376.5 and 37.2 MHz for ^{19}F and ^{91}Zr, respectively. Because of the strong reactivity of molten fluorides at high temperature, we used the laser heating system developed in our laboratory, in combination with boron nitride (BN) airtight crucibles. This system has already been used for different molten fluorides and has proved to be well adapted.[20–22]

Samples were packed in crucibles made in pure boron nitride (BN purchased from MCSE, France), air tightly closed. We used a single pulse sequence to acquire ^{19}F and ^{91}Zr signals. For the ^{19}F, we used a pulse excitation of 7.5 μs, with a recycle delay of 500 ms, and for ^{91}Zr, we used a pulse excitation of 40 μs, with a recycle delay of 250 ms. ^{91}Zr and ^{19}F chemical shifts were referenced relative to a saturated solution of $Zr(C_5H_5Cl)_2$ in CH_2Cl_2 at 0 ppm and to pure $CFCl_3$, respectively.

For each experiment, the samples were kept around 1 h in the liquid phase to obtain both ^{19}F and ^{91}Zr spectra. Samples were heated with two CO_2 lasers ($\lambda = 10.6$ μm), one located underneath and the other above the magnet, to minimize the temperature gradient inside the crucible. We heated between 590 and 1120 K, corresponding to 20−30 K above the different melting points given by the phase diagrams.[18,19] Signals obtained are sharp and Lorentzian and correspond to the average signature of the different species in the melt. It is important to notice that all these signals do not change when the temperature increases. All the NMR spectra were fitted with the DMfit software.[23]

B. EXAFS. Experimental EXAFS measurements were performed in transmission geometry at the K-edge of zirconium (17998 eV), with a double crystals Si (111) monochromator, on the BL27B beamline[24] of the Proton Factory (PF) in Tsukuba (Japan), and on the DIFFABS beamline on the SOLEIL synchrotron in Gif-Sur-Yvette (France). We studied the same $LiF-ZrF_4$ compositions as for NMR measurements, ranging from 0 to 50 mol % ZrF_4. For each composition, we prepared pellets from appropriate mixtures of boron nitride and metal fluorides. The proportion of each constituent was calculated by taking into account the absorption coefficient relative to the pellet thickness and using the Absorbix software.[25]

Pellets of 1 cm diameter are pressed under 5 tons cm^{-2}, to obtain a thickness of 400 μm. Pellets are packed inside two plates made of pyrolytic boron nitride (PBN), tightly closed with 8 screws. This system was initially developed for EXAFS measurements in molten $AF-MF_3$ systems ($A^+ = Li^+, Na^+, K^+$; $M^{3+} = Y^{3+}, La^{3+}, Lu^{3+}$).[26–28] The cell[29] can be heated in a furnace with a geometry adapted to the transmission mode. The heating chamber is cooled by water and the atmosphere inside is controlled by a helium gas flow (0.2 L min^{-1}).

On the BL27B beamline, the flux of incident and transmitted photons was detected by two ionization chambers filled in the N_2 and N_2-Ar (50%) mixture, respectively. The beam size was 1.5 mm vertically and 5 mm horizontally. Fixed time (1 s/point) scanning was performed in the energy range from 17.7 to 18.9 keV. To minimize the time of collection and to have a better energy resolution around the absorption edge, we subdivided this range in four areas (17.7−17.95 keV), (17.95−18.1 keV), (18.1−18.5 keV), (18.5−18.9 keV) by varying the energy step by 2, 0.5, 2, and 4 eV, respectively.

For the measurements on the DIFFABS beamline, we used two Si photodiodes as detectors and we reduced the beam spot

size to 930 × 170 (H × V μm^2). The linear coefficient of X-ray absorption was made on an energy range from 17.8 to 18.8 keV separated in three areas (17.8−17.9 keV; 17.9−18.5 keV; 18.5−18.8 keV) by using a step of 4 eV/s for the first and the third zone, and 2 eV/s for the second zone.

In both cases, the collection time of one scan is about 15 min. To obtain a good signal-to-noise ratio on the absorption data, we collected four scans in the liquid phase and two scans in the solid phases. The EXAFS oscillations were extracted by using Athena software.[30,31]

For each experiment, the samples were heated to 50 K above the melting temperature. We heated the melt with a 10 K/min heating rate and waited 10 min before acquisition to homogenize the liquid. As observed previously for the NMR experiments, the EXAFS oscillations do not change with the temperature when the system is molten. Furnaces used for the experiment are described by Matsuura et al.[32] and Bessada et al.[33]

C. Molecular Dynamics. We have used a molecular dynamics (MD) code in which the polarizable ion model is implemented. This code is dedicated to calculations in ionic liquids.[4,34] It allows us to generate via classical molecular dynamics calculations the trajectories of ions inside a periodically replicated simulation cell and then to extract the relevant physicochemical properties of the melt. The interaction potential consists of a sum of pairwise additive interactions supplemented with a many-body polarization term, as previously described by Salanne et al.[35−38] The various parameters involved in the interaction potential were constructed through a "force-fitting" procedure; they are listed in ref 35. Such a procedure has also been applied in the case of oxides.[39−41] To determine forces and dipoles of each ions, first-principles electronic structure calculations are performed for a given system using the plane waves density functional theory formalism. Parameters of the potential are then obtained by minimizing the difference between the forces and dipoles predicted by the model to the first-principles calculated ones.

MD simulations were then carried out on molten $LiF-ZrF_4$ mixtures. Calculations were performed at the same temperatures used for EXAFS measurements, and also at a constant temperature of 1125 K. In each case, the systems were first equilibrated in the *NPT* ensemble with a pressure fixed to 0 GPa. Second, *NVT* ensemble runs were realized at the equilibrated cell volume. The method used to enforce *NVT* ensemble sampling is the Nosé−Hoover chain thermostat method.[42,43] Simulation times were 200 ps, with a time step of 0.5 fs. The number of atoms, box sizes, and temperatures used for these calculations are listed in Table 1.

D. EXAFS Computation by FEFF. The EXAFS function $\chi(k)$ was obtained from an ab initio calculation, by using the FEFF8[44] code from the Cartesian positions of Li^+, F^-, and Zr^{4+} ions given by the MD simulation. To determine this function, it is necessary to define, among several parameters (absorption edge, amplitude reduction factor, etc.), the maximal length of the scattering paths that contributes to the total EXAFS signal. This cutoff distance was fixed to 8 Å: Beyond this value, the paths give a negligible contribution to the total EXAFS signal.

FEFF uses an ab initio self-consistent real space multiple scattering approach for clusters of atoms ($Z < 99$) including the core−hole effects. Calculations are based on an all-electron real space relativistic Green's function formalism with no symmetry requirements. The method combines both full multiple scattering based on Lanczos algorithms and high-order path expansion based on the Rehr−Albers multiple scattering formalism. However, the multiple scattering contributions are negligible in the disordered systems of interest here. All the FEFF computations were therefore performed considering only single backscattering paths (Nleg = 2).

The Debye−Waller factor in the EXAFS standard formula is substituted by accumulation of FEFF calculations on atomic configuration data. Every 10 time steps, a FEFF calculation is performed on a new frozen atomic arrangement. The final EXAFS curve is the average of FEFF computations on 10 000 up to 20 000 different atomic configurations. A further increase of the number of atomic configurations did not improve the quality of the spectra.

TABLE 1: Molecular Dynamics Simulations Conditions[a]

mol % ZrF_4	N_{F^-}	$N_{Zr^{4+}}$	N_{Li^+}	F/Zr ratio	L (Å)	T (K)
5	260	11	216	23.6	18.2	1120
10	247	19	171	13.0	17.6	1100
10	247	19	171	13.0	17.6	1125
15	222	23	130	9.7	16.8	1070
15	222	23	130	9.7	16.9	1125
21	273	35	133	7.8	17.6	970
21	273	35	133	7.8	17.9	1125
25	287	41	123	7.0	18.1	1050
25	287	41	123	7.0	18.3	1125
30	367	58	135	6.3	19.5	970
30	367	58	135	6.3	19.7	1125
35	340	58	108	5.9	19.2	920
35	340	58	108	5.9	19.4	1125
40	297	54	81	5.5	18.0	870
40	297	54	81	5.5	18.5	1125
45	272	52	64	5.2	17.4	840
45	272	52	64	5.2	17.7	1125
50	290	58	58	5.0	17.5	800
50	290	58	58	5.0	18.0	1125

[a] L is the cubic simulation cell edge length.

III. Results

A. Coordination Number of Zirconium. ^{91}Zr has a nuclear spin $I = {}^5/_2$ associated with a large nuclear quadrupolar moment (-0.176×10^{-28} m^2)[45] and is therefore subject to strong quadrupolar interactions. This leads to some difficulties in acquiring spectra in solid phases.[46] In a previous study[47] we have performed high-resolution solid state NMR of zirconium in selected and well-crystallized compounds to build an empirical correlation between the ^{91}Zr chemical shift and the local structure around the zirconium atoms. In the solid the signals are very broad and require some specific techniques to be observed. In the molten phase, the quadrupolar interaction is totally averaged and its effects are vanished: the signal is sharp and detectable in a few scans.

All high-temperature NMR spectra obtained in the melts consisted of a single resonance Lorentzian line. This means either that one single species is present or that there is a rapid chemical exchange between different fluorozirconate ($[ZrF_x]^{4-x}$) species present in the melt: In that case, the position of the resonance line, the chemical shift, corresponds to the weighted average of the isotropic chemical shifts of these different species. Knowing the values of the individual isotropic chemical shift would allow quantifying the relative amount of the different species in the melt. Here, this is not possible: We can only extract the average coordination number (CN) of the Zr^{4+} ion, using the empirical correlation provided in ref 46.

The data provided in Figure 1a consists in the first reported ^{91}Zr NMR spectra in a molten phase. The temperature ranges from 800 to 1120 K, depending on the composition. The low signal-to-noise ratio visible on these high-temperature spectra

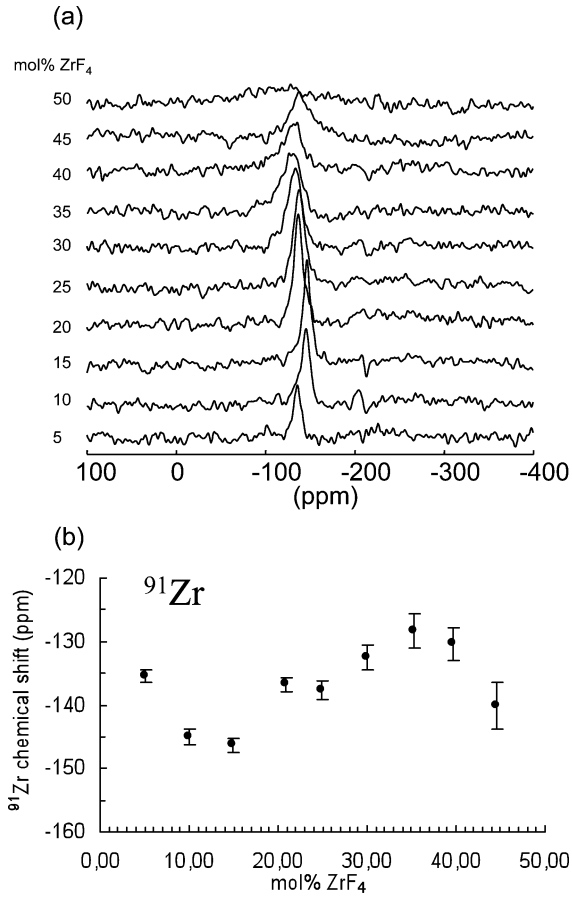

Figure 1. (a) ^{91}Zr NMR spectra in LiF−ZrF_4 melts (temperature range extended from 800 to 1120 K depending on the melting temperature at each composition). (b) ^{91}Zr chemical shifts plotted as a function of the proportion of ZrF_4.

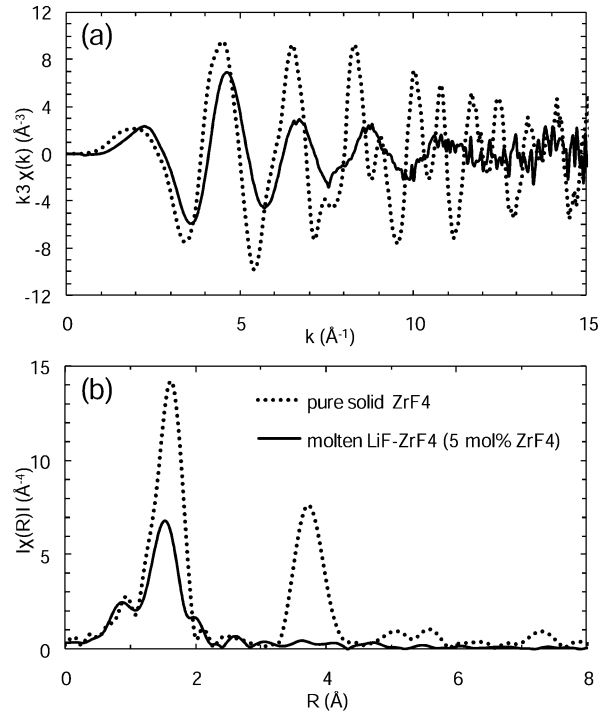

Figure 2. Comparison between (a) EXAFS oscillations and (b) Fourier transform of these EXAFS oscillations obtained at the K-edge of zirconium in solid β-ZrF_4 at room temperature (dotted black line) and in molten LiF−ZrF_4 (5 mol % ZrF_4) at 1120 K (full black line).

is due to the properties of ^{91}Zr, which has a relatively weak natural abundance (11.23%) and a low gyromagnetic ratio (3.958 MHz. T^{-1}). Because of the volatility of ZrF_4, we have tried to find a compromise between the heating duration in the melt and the quality of the signal. So we limited the acquisition time to around 15 min to reduce the overall duration of the experiment and the possible evaporation of the sample and thus the evolution of the composition.

^{91}Zr chemical shifts extracted from the NMR spectra are plotted as a function of the ZrF_4 molar percentage in Figure 1b. We note that the variation of the signal with ZrF_4 content is relatively complex and nonmonotonous, even if the domain of chemical shifts measured over the entire range of compositions extended over 25 ppm only. In ref 46, we established that such ^{91}Zr chemical shifts between −125 and −150 ppm correspond most probably to an average 7-fold coordination for zirconium ion.

To obtain more quantitative information on the CN of zirconium, we carried out EXAFS experiments at the K-edge of Zr (17.9 keV). The EXAFS data were obtained for the solid (at room temperature before and after heating) and for the molten compounds. We report in Figure 2a the EXAFS oscillations of the solid β-ZrF_4 and the molten salt LiF−ZrF_4 (with 5 mol % ZrF_4). Contrary to the case of the solid compound, the signal of the liquid is characteristic of a poorly structured environment. The important damping of the signal is due to the increase of the disorder induced by the thermal effects. The shift indicates a contraction of the distances between the absorber atom (Zr) and its firsts neighbors (F). This effect can be seen on the Fourier transform of the EXAFS signal (Figure 2b) by a decrease of the amplitude of the first peak and a shift toward smaller distances. The disappearance of peaks at higher distance is due to the absence of a long distance order in the liquid. We also note that in the liquid, the phase, and the amplitude of the oscillations do not change drastically with composition (Figure 3).

For highly disordered materials, performing a simple Fourier transformation of the EXAFS oscillations is not suitable to extract reliable structural parameters.[48–50] Okamoto proposed a procedure adapted to the case of molten salts, based on the combination of molecular dynamics and the EXAFS simulation code FEFF 8.[51,52] In this procedure, the atomic configuration data obtained from the MD are directly used as input data in the FEFF code, to calculate EXAFS oscillations, as depicted in the experimental section. The Debye−Waller factor and the anharmonic vibration effect are substituted by accumulating the MD steps. The crucial point of this method is to have a reliable interaction potential that allows a correct description of the structure of the ionic liquid at high temperature.

To check the validity of our interaction potential for describing the structure of the LiF−ZrF_4 system, we compared the calculated oscillations with the experimental ones. As shown in Figure 3, calculations reproduce with a satisfactory level the amplitude and the phase of the experimental signals obtained in the liquid state; this is particularly true at low ZrF_4 content. For concentrations higher than 40 mol % ZrF_4, differences on the amplitude of the signal start to be observed.

The MD simulations therefore give an accurate description of the structure of the salt in the molten state. By analyzing directly the results of the molecular dynamics simulations, we extracted the structural parameters, such as first-neighbor distance and CNs. The latter are determined by counting the number of F^- ions located at a distance shorter than 2.48 Å (the first minimum of the Zr−F radial distribution function) from

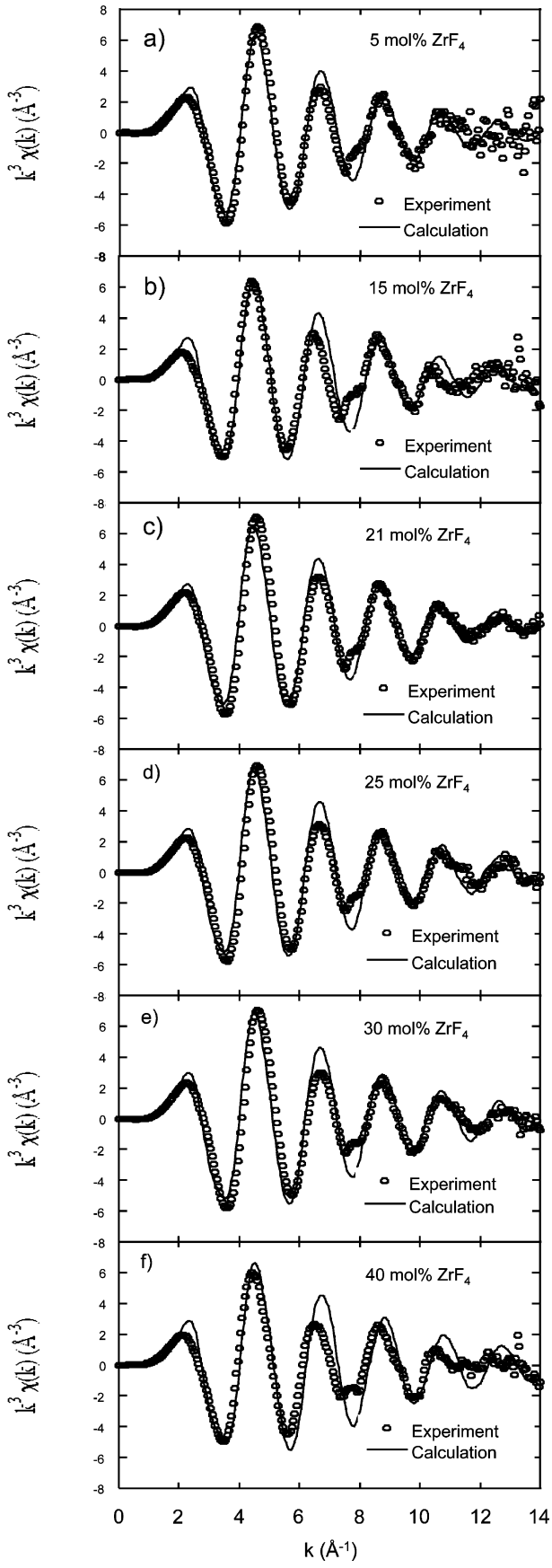

Figure 3. Experimental (dotted line) and calculated (full line) EXAFS oscillations in $LiF-ZrF_4$: (a) 95−5 mol % at 1120 K; (b) 85−15 mol % at 1070 K; (c) 79−21 mol % at 970 K; (d) 75−25 mol % at 1050 K; (e) 70−30 mol % at 970 K; (f) 60−40 mol % at 870 K.

TABLE 2: Structural Parameters Extracted from MD Simulations at Temperatures 50 K above the Melting Temperature[a]

mol % ZrF_4	% CN 6	% CN 7	% CN 8	average CN	d_{Zr-F} (Å)
5	20.6	62.9	16.4	7.0	2.061
10	21.9	63.6	14.3	6.9	2.060
15	22.3	62.8	14.8	6.9	2.056
21	22.0	61.2	16.6	6.9	2.052
25	38.5	51.3	10.0	6.7	2.041
30	42.5	47.8	9.4	6.6	2.039
35	67.9	27.1	4.9	6.4	2.018
40	41.7	46.0	12.0	6.7	2.037
45	34.5	48.9	16.1	6.8	2.045
50	21.1	51.3	26.3	7.0	2.065

[a] Uncertainty for d_{Zr-F} is ±0.002 Å.

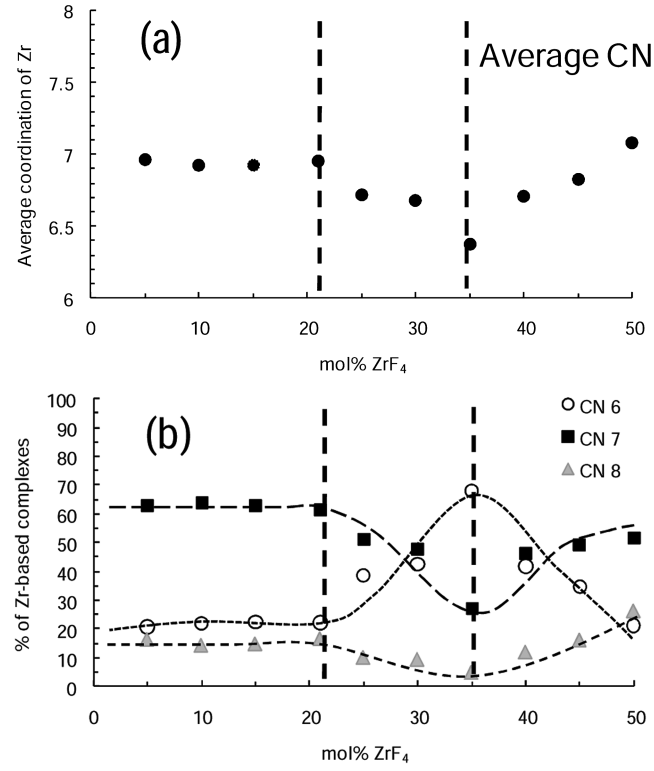

Figure 4. (a) Average coordination number of the zirconium ion and (b) evolution of the percentages of the different Zr-based complexes coexisting in the melts (circles, $[ZrF_6]^{2-}$; squares, $[ZrF_7]^{3-}$; triangles, $[ZrF_8]^{4-}$) in the molten $LiF-ZrF_4$ system, from 0 to 50 mol % ZrF_4, at temperatures 50 K above the melting temperature.

a Zr^{4+}. These quantities are reported in Table 2 for the whole range of compositions, together with the content in 6-, 7-, and 8-fold coordinated zirconium; no other CNs were observed within this study. The CN data are also plotted versus the molar percentage of ZrF_4 in Figure 4a. We observe a strong similarity between the CN evolution and the ^{91}Zr NMR chemical shift one, provided in Figure 1b.

In Figure 4a we underlined the existence of three domains for the calculated average CN. It is stable in the first domain up to the eutectic composition (21 mol % ZrF_4), and then decreases between 21 and 35 mol %. Above 35 mol % the average coordination number increases toward the coordination of zirconium in solid ZrF_4 (CN = 8). We notice that the anomalous points of the evolution of the CN correspond to some particular compositions for the liquidus curve of the phase diagram. Such a similarity was already observed in the $LiF-PbF_2$ system.[53]

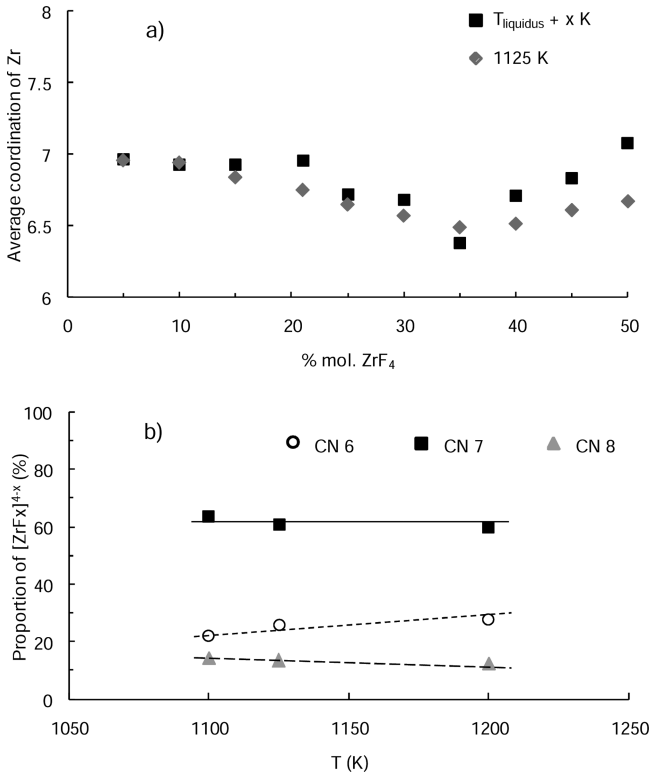

Figure 5. (a) Comparison of the average coordination number of the zirconium ion at temperatures 50 K above the melting temperature and at 1125 K from 0 to 50 mol % ZrF_4 and (b) evolution of the percentages of the different Zr-based complexes coexisting in the melts (circles, $[ZrF_6]^{2-}$; squares, $[ZrF_7]^{3-}$; triangles, $[ZrF_8]^{4-}$) in the sample containing 10 mol % ZrF_4.

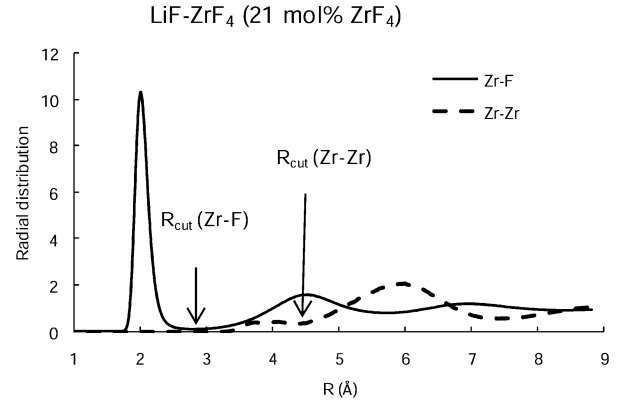

Figure 6. Partial radial distribution functions $g_{Zr-F}(r)$ and $g_{Zr-Zr}(r)$ of molten LiF−ZrF_4 (21 mol % ZrF_4) calculated in the MD simulations. Cutoff radii used to calculate the number of bridging fluorides: R_{cut}(Zr−F) = 2.84 Å and R_{cut}(Zr−Zr) = 4.36 Å.

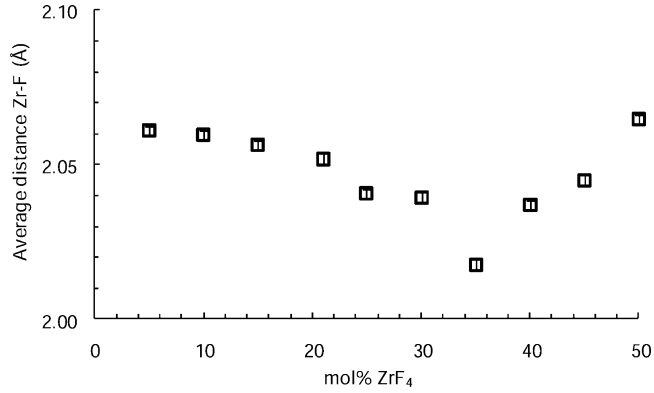

Figure 7. Evolution of the average Zr−F distance with addition of ZrF_4.

Results from molecular dynamics depict an evolution of the average CN, which is due to the coexistence of three different complexes in the melt: $[ZrF_6]^{2-}$, $[ZrF_7]^{3-}$, and $[ZrF_8]^{4-}$. Figure 4b shows the evolution of the proportion of these three different complexes with addition of ZrF_4. From 0 to 50 mol % ZrF_4, the predominant species is always $[ZrF_7]^{3-}$, except at 35 mol %. For this composition, which corresponds to the Li_2ZrF_6 compound in the solid state, the major species is $[ZrF_6]^{2-}$. The $[ZrF_8]^{4-}$ species is relatively stable on the entire domain of composition but, as $[ZrF_7]^{3-}$, increases from 35 mol %.

The assumption of the coexistence of these three anionic complexes was proposed by different authors, using experimental and theoretical approaches. Spectroscopic techniques[14,15,54] and physical thermodynamic models[16,17] suggest strong acid−base reactions, involving transfers of fluoride ions to zirconium. These transfers would be at the origin of the formation of anionic complexes with 6- to 8-fold coordination for zirconium. Hatem et al.[16] explained the large exothermic enthalpies measured in this system by the presence of these three species. This enthalpy of mixing is an important macroscopic thermodynamic parameter, giving information on the energy modifications that occur between particles during the formation of the mixture. It is also a useful tool to give information on the microscopic structure of the liquid, provided that a relevant model is introduced to analyze the thermodynamic data. In Hatem's work, the measured minimum of mixing enthalpy corresponds to 40 mol % ZrF_4, and to a F/Zr ratio of 6. This result is interpreted as the signature of the formation of $[ZrF_6]^{2-}$ octahedra. It is in agreement with our results, which show that the octahedral configuration of zirconium is very abundant in the liquid phase at a similar composition. In the case of rich LiF compositions, which correspond to a F/Zr ratio higher than 6 (less than 40 mol % ZrF_4), the interpretation of Raman spectroscopy data[14] opened the possibility of the formation of $[ZrF_7]^{3-}$ and $[ZrF_8]^{4-}$. Combined MD/EXAFS results support this conclusion, with an important predominance of 7-fold coordinated species: The $[ZrF_7]^{3-}/[ZrF_8]^{4-}$ ratio is of about 4 for the lower amounts of Zr (0−21 mol % ZrF_4). At higher content of ZrF_4 (F/Zr ratio smaller than 6), Grande et al. also introduced $[ZrF_7]^{3-}$ and $[ZrF_8]^{4-}$ anionic complexes in their model, to reproduce the macroscopic thermodynamic data (phase diagram and heat of mixing).[17] Our results are in good agreement with this assumption, and we get a $[ZrF_7]^{3-}/[ZrF_8]^{4-}$ ratio of about 2 for 50 mol % ZrF_4.

To unpick the temperature effects from the composition ones, we have performed simulations of the different systems at the same temperature, namely $T = 1125$ K. The corresponding CNs are displayed in Figure 5a, on which we also reproduce the values from Figure 4a. The evolution is similar in both cases up to 10 mol % ZrF_4. Above this value, a small deviation of about 3% is observed between both curves. Figure 5b presents the proportions of the three Zr-based complexes for the composition containing 10 mol % ZrF_4 at 1100, 1125 and 1200 K. It clearly appears that the proportions do not strongly change with the temperature, showing that the composition of the system is the important quantity that determines the speciation.

B. Average Zr−F Distances. To determine the average Zr−F distance, we fitted the first peak of the Zr−F radial distribution (Figure 6) by using an exponentially modified gaussian (EMG) function.[55] The EMG model convolutes a Gaussian function with an exponential one. It provides the best

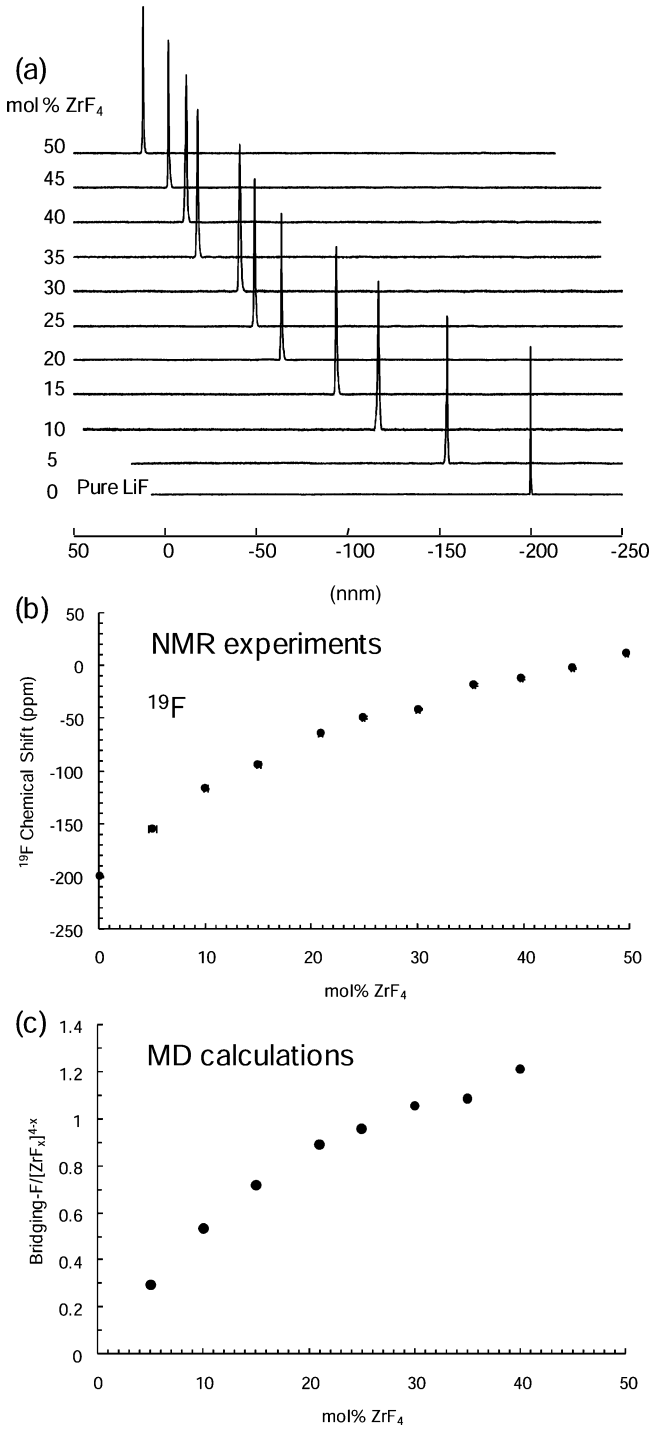

Figure 8. (a) ^{19}F NMR spectra in $LiF-ZrF_4$ melts (temperature range extended from 800 to 1120 K depending on the melting temperature at each composition), (b) chemical shift of ^{19}F and (c) average number of bridging fluorides per Zr-based complexes, all plotted as a function of the proportion of ZrF_4.

results to fit the asymmetric peaks in our case. The determination of the main peak parameters is based on the estimation of the four statistical moments (average distance, variance, skewness, and kurtosis) from the peak shape model in four parameters. According to the fit, we observe a contraction of the distances between Zr^{4+} and F^- (d_{Zr-F}) from the solid to the liquid: the average distance ranges between 2.037 and 2.065 ± 0.002 Å (Table 2) in the molten phase, versus 2.211 Å in the solid.[56]

In Figure 7 is reported the evolution of d_{Zr-F} as a function of the molar percentage of ZrF_4. For steric reasons, the average distance Zr−F is closely related to the number of fluoride ions in the zirconium first solvation shell, and so the shape of the figure is similar to the one obtained for the zirconium average CN (Figure 4a). Again, the global minimum of the curve corresponds to a composition of 35 mol % because of the predominance of $[ZrF_6]^{2-}$ complexes.

C. Bridging Fluorides. ^{19}F NMR spectra obtained in molten $LiF-ZrF_4$ mixtures are presented in Figure 8a. The temperature range is the same as for ^{91}Zr experiments. The signal-to-noise ratio is excellent compared to the previous ^{91}Zr spectra. ^{19}F is 100% abundant, has a nuclear spin of $^1/_2$, and has a high Larmor frequency (376.5 MHz at 9.4 T). These NMR properties explain the very good quality of the signals. At each composition, we controlled that the signal did not change with temperature. In Figure 8b we report the ^{19}F chemical shift evolution with ZrF_4 content. It increases progressively from −200 ppm in pure LiF to 12 ppm for the melt containing 50 mol % ZrF_4.

This evolution is very similar to the trend already observed in the case of rare earth fluorides alkali fluorides systems ($AF-RF_3$) and for the $AF-ThF_4$ system ($A^+ = Li^+$, Na^+, or K^+).[21,22] The evolution is monotonous and nonlinear with composition: it is due to the existence of three different fluoride types. At high LiF content, fluoride ions are mainly free. When ZrF_4 is added, they start to be involved in zirconium-based complexes $[ZrF_x]^{4-x}$ and for higher amounts of ZrF_4, connections are formed between $[ZrF_x]^{4-x}$ complexes by bridging fluorides.

We calculated from the MD simulations the number of bridging fluorides. In Figure 6, the Zr−Zr radial distribution function is superimposed with the Zr−F partial one. The first peak shows a small shoulder for distances lower than 4.36 Å, which is less than the length of two Zr−F bonds, indicating pairs of Zr ions linked by common F^- anions. We used a geometrical criterion to determine the number of so-formed bridging fluorides. We chose to define a Zr−F−Zr bond when the distance between two Zr^{4+} is shorter than 4.36 Å and a given F^- ion is at a distance shorter than the first minimum in the Zr−F radial distribution function (2.84 Å) to both of them. These two characteristic distances are indicated by arrows in Figure 7. In Figure 8c is shown the evolution of the average number of bridging fluorides upon addition of ZrF_4. This evolution deduced from the calculations is in agreement with the evolution of the chemical shift in NMR experiments. It shows that the liquid becomes partly associated with addition of ZrF_4

IV. Conclusion

We investigated the local structure of zirconium and fluoride ions in the molten $LiF-ZrF_4$ system by the combination of high-temperature NMR and EXAFS experiments with MD simulations. From ^{91}Zr high-temperature NMR an average coordination number of 7 has been determined for the zirconium on all domains of composition. The EXAFS experimental data at the K-edge of zirconium were well reproduced by the combination of MD simulations and FEFF computations. We can therefore conclude on the coexistence of three different complexes in the melt: $[ZrF_6]^{2-}$, $[ZrF_7]^{3-}$, and $[ZrF_8]^{4-}$. The major species present in the melt is $[ZrF_7]^{3-}$ for all compositions, except at 35 mol % ZrF_4 for which a singularly high amount of $[ZrF_6]^{2-}$ is observed. The existence of such a change in the coordination number around Zr, as the mixture composition is changed, is in itself a result that goes against conventional wisdom in these molten salt systems, which holds that highly charged ions have a preferred coordination number that is maintained. Such a result is of high importance, since speciation properties are often used as an input in thermodynamic models that are developed for

engineering purposes.[57,58] In agreement with the ^{19}F high-temperature NMR experiments, MD calculations also highlight an increase of the number of bridging fluorines between zirconium fluorides complexes with the addition of ZrF_4.

Acknowledgment. We thank the CNRS Programme PCR ANSF and the Regional Council of the Region Centre for financial support. We also thank Dr. Dominique Thiaudiere, Dr. Solenn Réguer (SOLEIL Synchrotron), and Mr. Masahiko Numakura (JAEA, Japan) for their help in our experiments on the Diffabs and BL27 beamlines in France and Japan. We thank Emmanuel Véron and Sandra Ory (CEMHTI, Orléans) for XRD and DSC measurements and Dr. Anne-Laure Rollet for her contribution to the development of all the instrumentation. These EXAFS data were obtained by the experiments under the proposal numbers 2006G318 and 2008G065 (PF/KEK, Japan) and 20060237 and 20080276 (SOLEIL, France).

References and Notes

(1) Photiadis, G.; Papatheodorou, G. *J. Chem. Soc., Dalton Trans.* **1998**, 981–989.
(2) Photiadis, G.; Papatheodorou, G. *J. Chem. Soc., Dalton Trans.* **1999**, 3541–3548.
(3) Hutchinson, F.; Rowley, A.; Walters, M.; Wilson, M.; Madden, P.; Wasse, J.; Salmon, P. *J. Chem. Phys.* **1999**, *111*, 2028.
(4) Hutchinson, F.; Wilson, M.; Madden, P. *Mol. Phys.* **2001**, *99*, 811.
(5) Lacassagne, V.; Bessada, C.; Florian, P.; Bouvet, S.; Ollivier, B.; Coutures, J.-P.; Massiot, D. *J. Phys. Chem. B* **2002**, *106*, 1862.
(6) Watanabe, S.; Adya, A.; Okamoto, Y.; Umesaki, N.; Honma, T.; Deguchi, H.; Horiuchi, M.; Yamamoto, T.; Nogushi, S.; Takase, K.; et al. *J. Alloys Compd.* **2006**, *408−412*, 71.
(7) Brun, C. L. *J. Nucl. Mater.* **2007**, *360*, 1.
(8) Vergnes, J.; Lecarpentier, D. *Nucl. Eng. Des.* **2002**, *216*, 43.
(9) van der Meer, J.; Konings, R. *J. Nucl. Mater.* **2007**, *360*, 16.
(10) Rosenthal, M.; Haubenreich, P.; McCoy, H.; McNeese, L. *At. Energy Rev.* **1971**, *9*, 601.
(11) Pherson, H. M. *Nucl. Sci. Eng.* **1985**, *90*, 374.
(12) Mathieu, L.; Heuer, D.; Brissot, R.; Garzenne, C.; Brun, C. L.; Lecarpentier, D.; Liatard, E.; Loiseaux, J.; Meplan, O.; Merle-Lucotte, E.; et al. *Prog. Nucl. Energy* **2006**, *48*, 664.
(13) Delpech, S.; Merle-Lucotte, E.; Heuer, D.; Allibert, M.; Ghetta, V.; Le-Brun, C.; Doligez, X.; Picard, G. *J. Fluorine Chem.* **2009**, *130*, 11.
(14) Toth, L.; Quist, A.; Boyd, G. *J. Phys. Chem.* **1973**, *77*, 1384.
(15) Dracopoulos, V.; Vagelatos, J.; Papatheodorou, G. *J. Chem. Soc., Dalton Trans.* **2001**, 1117–1122.
(16) Hatem, G.; Tabaries, F.; Gaune-Escard, M. *Thermochim. Acta* **1989**, *149*, 15.
(17) Grande, T.; Aasland, S.; Julsrud, S. *J. Am. Ceram. Soc.* **1997**, *80*, 1405.
(18) Dugat, P.; El-Ghozzi, M.; Metin, J.; Avignant, D. *J. Solid State Chem.* **1995**, *120*, 187.
(19) Benes, O.; Konings, R. *J. Alloys Compd.* **2008**, *452*, 110.
(20) Nuta, I.; Bessada, C.; Veron, E.; Matzen, G. *C. R. Chim.* **2004**, *7*, 395.
(21) Bessada, C.; Rollet, A.; Rakhmatullin, A.; Nuta, I.; Florian, P.; Massiot, D. *C. R. Chim.* **2006**, *9*, 374.
(22) Bessada, C.; Rakhmatullin, A.; Rollet, A.; Zanghi, D. *J. Nucl. Mater.* **2007**, *360*, 43.
(23) Massiot, D.; Fayon, F.; Capron, M.; King, I.; Le Calvé, S.; Alonso, B.; Durand, J.-O.; Bujoli, B.; Gan, Z.; Hoatson, G. *Magn. Reson. Chem.* **2002**, *40*, 70.
(24) Konishi, H.; Yokoya, A.; Shiwaku, H.; Motohashi, H.; Makita, T.; Kashihara, Y.; Hashimoto, S.; Harami, T.; Sasaki, T.; Maeta, H.; et al. *Nucl. Instrum. Methods Phys. Res. A* **1996**, *372*, 322.
(25) Michalowicz, A.; Charlier, C. Absorbix: Programme de calcul des coefficients d'absorption, http://www.icmpe.cnrs.fr/spip.php?article578.
(26) Rollet, A.; Bessada, C.; Rakhmatullin, A.; Auger, Y.; Melin, P.; Gailhanou, M.; Thiaudiere, D. *C. R. Chim.* **2004**, *7*, 1135.
(27) Rollet, A.; Rakhmatullin, A.; Bessada, C. *Int. J. Thermophys.* **2005**, *26*, 1115.
(28) Bessada, C.; Rakhmatullin, A.; Rollet, A.-L.; Zanghi, D. *J. Fluorine Chem.* **2009**, *130*, 45.
(29) Rollet, A.; Bessada, C.; Auger, Y.; Melin, P.; Gailhanou, M.; Thaudiere, D. *Nucl. Instrum. Methods Phys. Res. B* **2004**, *226*, 447.
(30) Newville, M. *J. Synchrotron Radiat.* **2001**, *8*, 322.
(31) Ravel, B.; Newville, M. *J. Synchrotron Radiat.* **2005**, *12*, 537.
(32) Matsuura, H.; Watanabe, S.; Akatsuka, H.; Okamoto, Y.; Adya, A. *J. Fluorine Chem.* **2009**, *130*, 53.
(33) Bessada, C.; Rollet, A.-L.; Zanghi, D.; Pauvert, O.; Thefany, C.; Matsuura, H.; Sitaud, B.; Solari, P. Actinide-XAS-2008 p. Publication of the OECD/Nuclear Energy Agency (2009).
(34) Madden, P.; Wilson, M. *Chem. Soc. Rev.* **1996**, *25*, 339.
(35) Salanne, M.; Simon, C.; Turq, P.; Madden, P. *J. Phys. Chem. B* **2008**, *112*, 1177.
(36) Salanne, M.; Simon, C.; Turq, P.; Madden, P. *J. Fluorine Chem.* **2009**, *130*, 38.
(37) Salanne, M.; Simon, C.; Groult, H.; Lantelme, F.; Goto, T.; Barhoun, A. *J. Fluorine Chem.* **2009**, *130*, 61.
(38) Benes, O.; Zeller, P.; Salanne, M.; Konings, R. *J. Chem. Phys.* **2009**, *130*, 134716.
(39) Aguado, A.; Madden, P. *Phys. Rev. B* **2004**, *70*, 245103.
(40) Norberg, S.; Ahmed, I.; Hull, S.; Marrocchelli, D.; Madden, P. *J. Phys.: Condens. Matter* **2009**, *21*, 215401.
(41) Marrocchelli, D.; Madden, P.; Norberg, S.; Hull, S. *J. Phys.: Condens. Matter* **2009**, *21*, 405403.
(42) Nosé, S. *Mol. Phys.* **1984**, *52*, 255.
(43) Martyna, G.; Klein, M.; Tuckerman, M. *J. Chem. Phys.* **1992**, *97*, 2635.
(44) Ankudinov, A.; Ravel, B.; Rehr, J.; Conradson, S. *Phys. Rev. B* **1998**, *58*, 007565.
(45) Kellõ, V.; Pyykkõ, P.; Sadlej, A.; Schwerdtfeger, P.; Thyssen, J. *Chem. Phys. Lett.* **2000**, *318*, 222.
(46) Bastow, T.; Smith, M.; Stuart, S. *Chem. Phys. Lett.* **1992**, *191*, 125.
(47) Pauvert, O.; Fayon, F.; Rakhmatullin, A.; Krämer, S.; Horvatić, M.; Avignant, D.; Berthier, C.; Deschamps, M.; Massiot, D.; Bessada, C. *Inorg. Chem.* **2009**, *48*, 8709.
(48) Filipponi, A. *J. Phys.: Condens. Matter* **2001**, *13*, R23.
(49) Ferlat, G.; Soetens, J.; Miguel, A. S.; Bopp, P. *J. Phys.: Condens. Matter* **2005**, *17*, S145.
(50) Ferlat, G.; Cormier, L.; Thibault, M.; Galoisy, L.; Calas, G.; Delaye, J.; Ghaleb, D. *Phys. Rev. B* **2006**, *73*, 214207.
(51) Okamoto, Y. *Nucl. Instrum. Methods Phys. Res. A* **2004**, *526*, 572.
(52) Okamoto, Y.; Suzuki, S.; Shiwaku, H.; Ikeda-Ohno, A.; Yaita, T.; Madden, P. *J. Phys. Chem. A* **2010**, *114*, 4664.
(53) Watanabe, S.; Matsuura, H.; Akatsuka, H.; Okamoto, Y.; Madden, P. *J. Nucl. Mater.* **2005**, *344*, 104.
(54) Wilmshurst, J. *J. Chem. Phys.* **1963**, *39*, 2545.
(55) Torres-Lapasio, J.; Baeza-Baeza, J.; Garcia-Alvarez-Coque, M. *Anal. Chem.* **1997**, *69*, 3822.
(56) Legein, C.; Fayon, F.; Martineau, C.; Body, M.; Buzare, J.-Y.; Massiot, D.; Durand, E.; Tressaud, A.; Demourgues, A.; Peron, O.; et al. *Inorg. Chem.* **2006**, *45*, 10636.
(57) Romero-Serrano, A.; Hallen-Lopez, M.; Zeifert, B.; Gomez-Yanez, C.; Hernandez-Ramirez, A. *J. Fluorine Chem.* **2009**, *130*, 336.
(58) Benes, O.; Konings, R. *J. Fluorine Chem.* **2009**, *130*, 22.

JP912195J